Chiral photonic crystals with an anisotropic defect layer

A. H. Gevorgyan* and M. Z. Harutyunyan
Yerevan State University, A. Manookian 1, 375025 Yerevan, Armenia
(Received 21 February 2007; published 4 September 2007)

In the present paper we consider some properties of defect modes in chiral photonic crystals with an anisotropic defect layer. We solved the problem by Ambartsumian's layer addition method. We investigated the influence of the defect layer thickness variation and its location in the chiral photonic crystal (CPC) and also its optical axes orientation, as well as of CPC thickness variation on defect mode properties. Variations of the optical thickness of the defect layer have its impact on the defect mode linewidth and the light accumulation in the defect. We obtain that CPCs lose their base property at certain defect layer thicknesses; namely, they lose their diffraction reflection dependence on light polarization. We also show that the circular polarization handedness changes from right-handed to left-handed if the defect layer location is changed, and therefore, such systems can be used to create sources of elliptically polarized light with tunable ellipticity. Some nonreciprocity properties of such systems are investigated, too. In particular, it is also shown that such a system can work as a practically ideal wide band optical diode for circularly polarized incident light provided the defect layer thickness is properly chosen, and it can work as a narrow band diode at small defect layer thicknesses.

DOI: 10.1103/PhysRevE.76.031701 PACS number(s): 42.70.Df, 42.70.Qs, 61.30.−v

I. INTRODUCTION

The photonic crystals (PCs) are a special class of artificial structures with periodic dielectric permittivity (these periods are on the order of the optical wavelengths) [1,2]. Such structures are a new type of artificial materials, having physical properties absent in natural dielectrics (as well as in semiconductors and metals) because their properties depend both on physical parameters of the substance of which they are consisted, and on the layer dimensions and structural periods. These structures are widely used in modern integral optics and optoelectronics, in laser and x-ray techniques, in the millimeter and submillimeter wavelength techniques, in the antenna technique and optical communications. The PCs make possible to control light wave propagation [1–4] and light wave localization in the presence of a defect in PC structure. The most important PCs' property is their spectrum zone structure, which is analogous to the energetic zone structure of electrons in semiconductors. The CPCs (cholesteric liquid crystals, chiral smectics, artificial chiral-made crystals [5–7], etc.) are of special interest. The main difference of the CPCs from usual PCs is the fact that the photonic band gap (PBG) in CPCs exists only for one circular polarization (at normal incident light) coinciding with the chiral medium helix sign. For these crystals circular Bragg reflection occurs between wavelengths $\lambda_1=\sigma n_o$ and $\lambda_2=\sigma n_e$, where σ is the pitch of helical structure, and $n_o=\sqrt{\epsilon_\parallel}$ and $n_e=\sqrt{\epsilon_\perp}$ are ordinary and extraordinary refractive indices of the locally uniaxial structure. Light with opposite circular polarization does not undergo a diffraction reflection.

The ideal PCs have many applications, but their doped versions are more useful, such as the doped semiconductors. Introduction of a defect into PC structure gives rise to additional resonance modes inside the PBG. Such defect modes are localized in defect positions and can be used to construct narrow band filters and low threshold lasers. Recently, the CPCs having various types of defects have been considered, namely, a thin layer of an isotropic substance installed between two CPC layers [8–13]; a defect caused by a helix phase jump on the boundary of two CPC layers [10,14–16]; a defect caused by a local change of the helix pitch [17–19]; and defects caused by spatially varying helix pitch [20–22]. The CPC with an anisotropic substance layer [23], three-layer system of two chiral-made thin layers with an anisotropic two-axes layer between them [24,25], is discussed and it was shown that this system's plane wave transmittance spectrum exhibits narrow-stop band characteristics in several wavelength regimes.

In this paper we theoretically investigate peculiarities of the defect modes in CPC with an anisotropic substance introduced between two layers of a chiral PC (Fig. 1) and have found out different features of such a system. The problem is solved by Ambartsumian's layer addition method [26], adjusted to the problems of this type [13,25,27]. Any CPC with an anisotropic defect can be considered as a three-layer system comprising two CPC layers and an anisotropic interlayer between them (i.e., as a Fabry-Perot resonator with diffraction mirrors and anisotropic medium between them).

Let us note that the concept of an anisotropic layer as a phase defect has been explicitly stated by Lakhtakia and Messier in [28] and, as it was shown very recently by Lakhtakia in [29], that an anisotropic defect layer can actually be a chiral PC, too.

II. THE METHOD OF ANALYSIS

Let us consider light propagation from the left through a multilayer system: CPC(1)-anisotropic dielectric layer (ADL)-CPC(2) (see Fig. 1). To solve this rather complicated problem we apply the effective layer addition method. This classical layer addition method was earlier developed for the

*agevorgyan@ysu.am

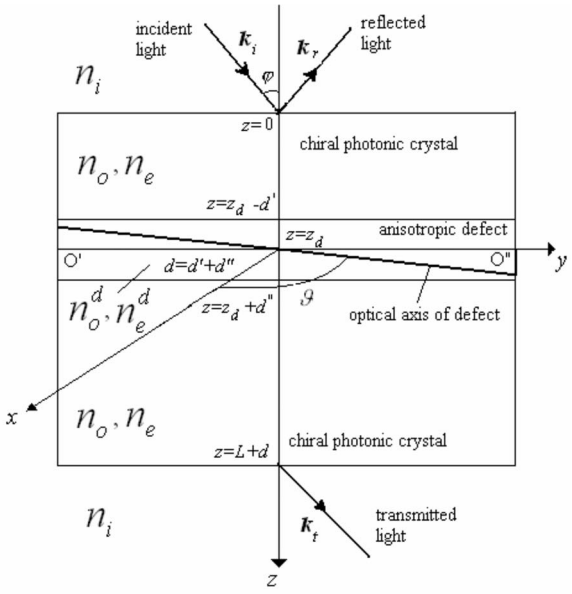

FIG. 1. Schematic diagram of a model CPC cell with an anisotropic defect.

solution of astrophysical problems of multiple scattering in turbid media [26]. The method has been developed for optical wave propagation through inhomogeneous media, in which it is necessary to use a more general description of optical effects in terms of "amplitude and phase" rather than simply "intensity" [27]. The advantage of this method is that introduction of the additional $\hat{S}$ and $\hat{P}$ matrices allows one to avoid the solution of extra equations when the system is more complicated, or when additional layers or radiating plane sources are introduced in the system, or when it is necessary to calculate the internal electrical field.

The amplitude of the electromagnetic field $\mathbf{E}_i$ is incident from the left on the system CPC(1)-ADL-CPC(2), and it gives rise to reflected $\mathbf{E}_r$ and transmitted $\mathbf{E}_t$ fields, respectively. The complex amplitudes of the *incident reflected* and *transmitted* waves with p and s linear polarizations are

$$\mathbf{E}_{i,r,t} = E^p_{i,r,t}\mathbf{n}_p + E^s_{i,r,t}\mathbf{n}_s = \begin{bmatrix} E^p_{i,r,t} \\ E^s_{i,r,t} \end{bmatrix}, \tag{1}$$

where $\mathbf{n}_p$ and $\mathbf{n}_s$ are the unit vectors of linear polarizations, and $E^p_{i,r,t}$ and $E^s_{i,r,t}$ are the corresponding amplitudes of the incident, reflected, and transmitted waves. The reflected and transmitted fields are related to the incident wave in the following way:

$$\begin{bmatrix} E^p_r \\ E^s_r \end{bmatrix} = \begin{bmatrix} R_{pp} & R_{ps} \\ R_{sp} & R_{ss} \end{bmatrix} \begin{bmatrix} E^p_i \\ E^s_i \end{bmatrix}, \quad \begin{bmatrix} E^p_t \\ E^s_t \end{bmatrix} = \begin{bmatrix} T_{pp} & T_{ps} \\ T_{sp} & T_{ss} \end{bmatrix} \begin{bmatrix} E^p_i \\ E^s_i \end{bmatrix}, \tag{2}$$

where $\hat{R}$ and $\hat{T}$ are the 2×2 Jones matrices of reflectance and transmittance correspondingly.

According to Ref. [27], the system consisted of two subsystems A and B, adjoined from "left to right" to each other through the "sewing" plane OO′ defines the reflection, $\hat{R}_{A+B}$, and transmission, $\hat{T}_{A+B}$, matrices of the composite system in terms of matrices A and B of the corresponding subsystems:

$$\hat{R}_{A+B} = \hat{R}_A + \tilde{\tilde{T}}_A \hat{S} \hat{T}_A,$$

$$\hat{T}_{A+B} = \hat{T}_B \hat{P} \hat{T}_A, \tag{3}$$

where

$$\hat{S} = \hat{R}_B [\hat{I} - \tilde{\tilde{R}}_A \hat{R}_B]^{-1},$$

$$\hat{P} = [\hat{I} - \tilde{\tilde{R}}_A \hat{R}_B]^{-1}. \tag{4}$$

The tildes in Eqs. (3) and (4) denote reflection-transmission properties of the subsystems when the wave is incident from the right. In particular, ADL or CPC or another subsystem, bordering with its both sides with the same medium, have Jones matrices for the incident light from the right and left connected by the expressions

$$\tilde{\tilde{T}} = \hat{F}^{-1} \hat{T} \hat{F},$$

$$\tilde{\tilde{R}} = \hat{F}^{-1} \hat{R} \hat{F}, \tag{5}$$

where $\hat{F} = \begin{pmatrix} 1 & 0 \\ 0 & -1 \end{pmatrix}$ for the linear base polarizations and $\hat{F} = \begin{pmatrix} 0 & 1 \\ 1 & 0 \end{pmatrix}$ for circular base ones.

Matrices $\hat{S}$ and $\hat{P}$ describe the resulting fields that arise in the dielectric layer on sewing plane OO′. The amplitude of electromagnetic field on the sewing plane for the light, propagating from the left is

$$\mathbf{E}_{\rightarrow} = \hat{P} \hat{T}_A \mathbf{E}_i, \tag{6}$$

and correspondingly for the light propagating from the right is

$$\mathbf{E}_{\leftarrow} = \hat{S} \hat{T}_A \mathbf{E}_i. \tag{7}$$

The total wave field arising in the dielectric layer on the sewing plane OO′ has the following form:

$$\mathbf{E}_{total} = (\hat{S} + \hat{P}) \hat{T}_A \mathbf{E}_i. \tag{8}$$

Substituting Eq. (4) into Eq. (3) we obtain the well-known *layers addition matrix equations*

$$\hat{R}_{A+B} = \hat{R}_A + \tilde{\tilde{T}}_A \hat{R}_B [\hat{I} - \tilde{\tilde{R}}_A \hat{R}_B]^{-1} \hat{T}_A,$$

$$\hat{T}_{A+B} = \hat{T}_B [\hat{I} - \tilde{\tilde{R}}_A \hat{R}_B]^{-1} \hat{T}_A, \tag{9}$$

which follow from the Stokes' and the Ambartsumian's *layers addition method*. The first method is the "successive reflections" [30] and the second one—"functional dependences," based on the invariance principle [26].

Using Eqs. (1)–(9) one can calculate the coefficients of reflection, $R = |E_r|^2/|E_i|^2$, and transmission, $T = |E_t|^2/|E_i|^2$, and the intensity of total field arising on the sewing plane OO′, $I = |E_{total}|^2/|E_i|^2$, which define the optical characteristics of the light propagation through the media with given parameters.

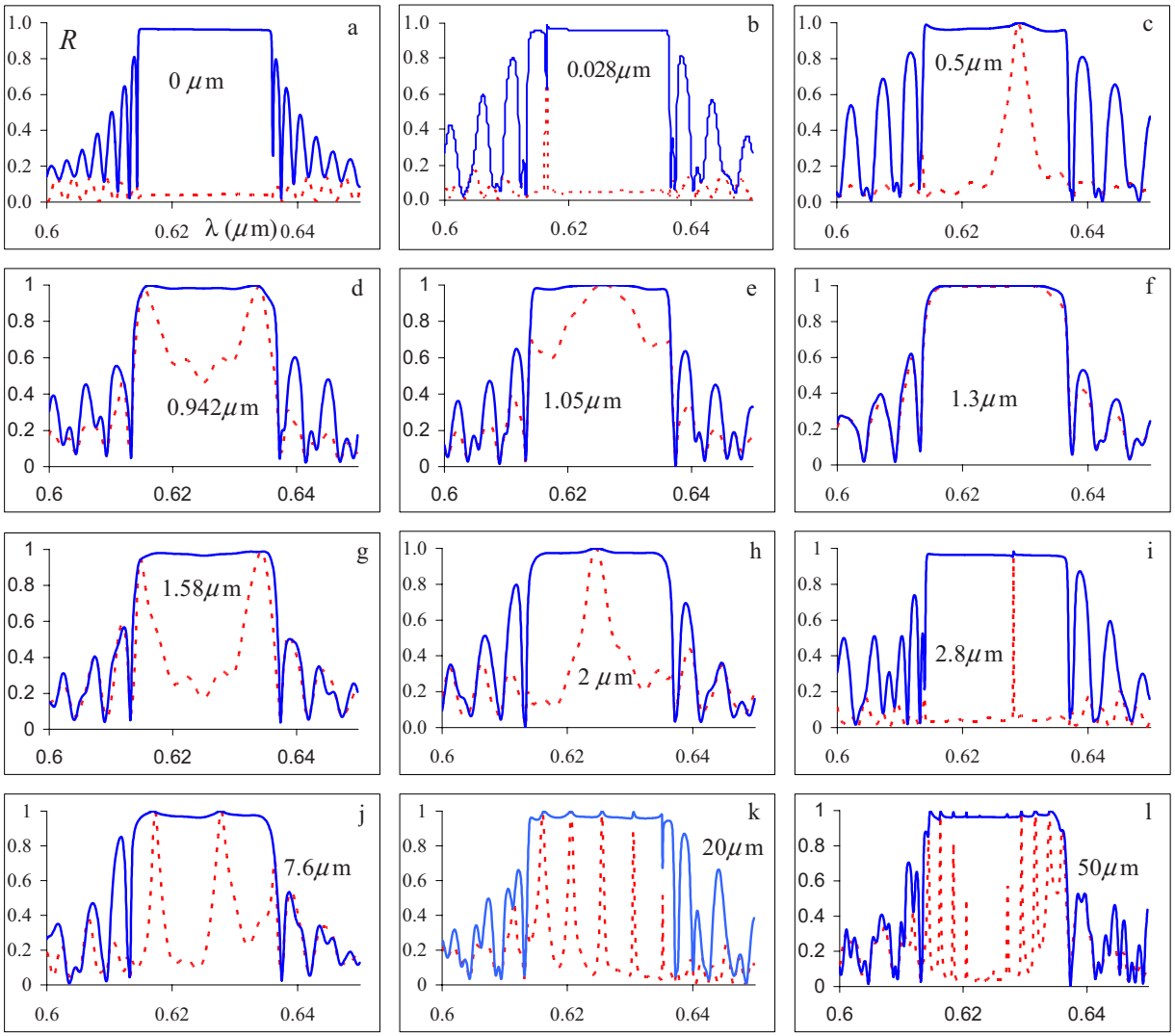

FIG. 2. (Color online) Plots of the reflection coefficient R versus wavelength λ for a right-handed CPC with a defect layer of various thicknesses d and for RCP (blue solid curve) and LCP (red dotted curve) light. Parameters are $n_e^d=1.746$, $n_o^d=1.522$, $L=100\sigma$, $\vartheta=0$.

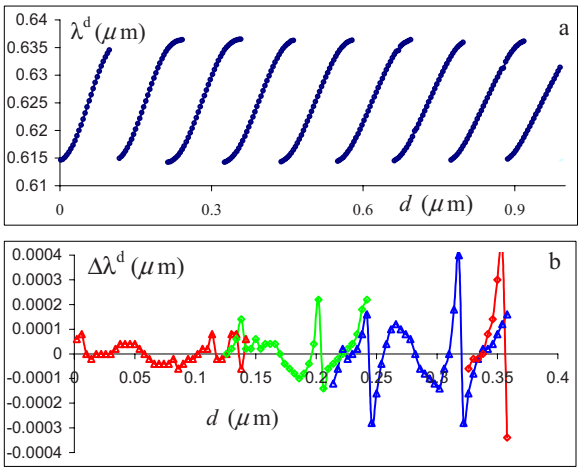

FIG. 3. (Color online) Plots of (a) defect mode wavelength λ^d and (b) defect mode wavelength difference for the RCP and LCP light versus defect layer thickness d. $n_e^d=1.449$, $n_o^d=1.342$. Other parameters are the same as in Fig. 2.

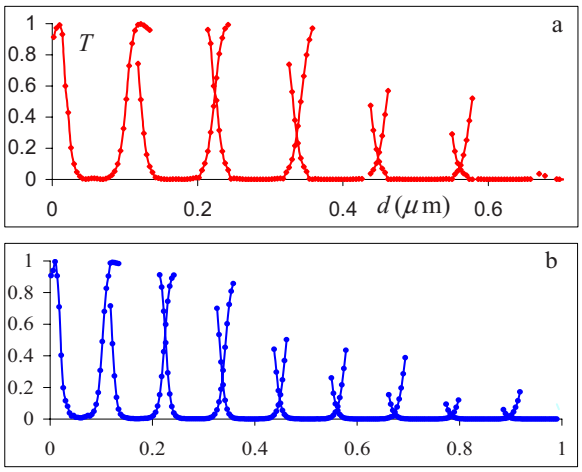

FIG. 4. (Color online) Plots of transmission coefficient T at the defect mode wavelength λ^d for the (a) RCP and (b) LCP light versus defect layer thickness d. Parameters are the same as in Fig. 3.

TABLE I. Parameters used in model calculations for a CPC with anisotropic defect layer.

	Symbol	Value
Refractive index of surroundings of cell	n_i	1.0
Local refractive indices (extraordinary and ordinary) of CPC	$n_e=\sqrt{\epsilon_\perp}$ $n_o=\sqrt{\epsilon_{\text{II}}}$	1.5133 1.4639
Refractive indices (extraordinary and ordinary) of defect layer	$n_e^d=\sqrt{\epsilon_\perp^d}$ $n_o^d=\sqrt{\epsilon_{\text{II}}^d}$	1.746, also 1.449 1.522, also 1.342
Pitch of CPC	σ	0.42 μm
PBG width	$\Delta\lambda=\sigma(n_e-n_o)$	0.6148–0.6356 μm
CPC layer thickness variation	ΔL	$0-500\sigma$
Defect layer thickness variation	Δd	0–50 μm
Defect position variation	Δz_d	$0-L$
Orientation angle of the optical axis of the defect	ϑ	0
Variation of ϑ	$\Delta\vartheta$	$0-\pi/2$
Angle of the incidence	φ	0

III. RESULTS AND DISCUSSION

In Fig. 2, the spectra of reflectance of the right-hand (the blue solid curve) and left-hand (the red dotted curve) circularly polarized light incidence for the above-mentioned system at various defect layer thicknesses are presented. The CPC screw is right handed. Figure 2(a) corresponds to the uniform CPC. As it is seen from the figure, defects give rise to localized defect modes—propagating in the forbidden band—and are manifested by sharp peaks and dips in the PBG in the reflection spectra. The defect mode of the nonresonance circular polarization (nondiffracting on the medium uniform structure, and of left circularly polarized in this case) of the incident wave reveals itself in the form of a peak in the reflection spectrum inside PBG, but that of the resonance polarization reveals itself both in the form of a peak and a dip in the reflection spectrum. And both modes practically have the same wavelength and the same reflection coefficients at the center of the peaks.

The defect mode has either a donor or an acceptor character depending on the defect layer thickness and its refraction coefficient. The defect mode wavelength increases from a minimum to a maximum band gap value if the defect layer thickness increases, and at both borders of PBG two defect modes appear [Figs. 2(d) and 2(g)], then the longer-wavelength mode leaves the PBG out and the other shorter-wavelength mode moves into the PBG as defect layer thickness increases further [Figs. 2(c), 2(e), and 2(h)]. A similar evolution pattern is observed if $\bar{n}^d=\sqrt{\frac{\varepsilon_\parallel^d+\varepsilon_\perp^d}{2}}$ increases. As it is shown in [8], analogous behavior takes place in the system with an isotropic defect. Let us note that in the general case the number of the defect modes in a one-dimensional (1D) PC depends on the optical thickness (i.e., on the product of the refraction index and the geometric thickness of the defect layer). In Fig. 3(a) the dependence of the defect mode wavelength λ^d on the layer thickness for the left circular polarization (LCP) is presented. As our calculations show, when there is a defect mode at the center of PBG, the defect layer optical thickness $\bar{n}^d d$ satisfies the relation

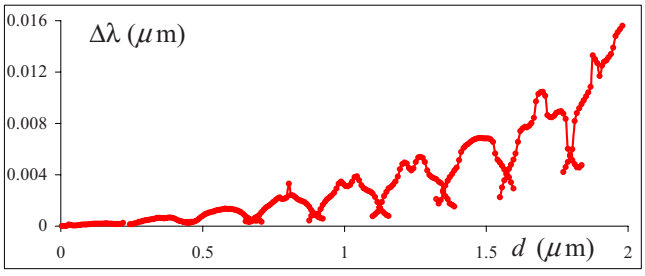

FIG. 5. (Color online) Plots of the defect line half-width $\Delta\lambda$ for the LCP light versus defect layer thickness d. Parameters are the same as in Fig. 3.

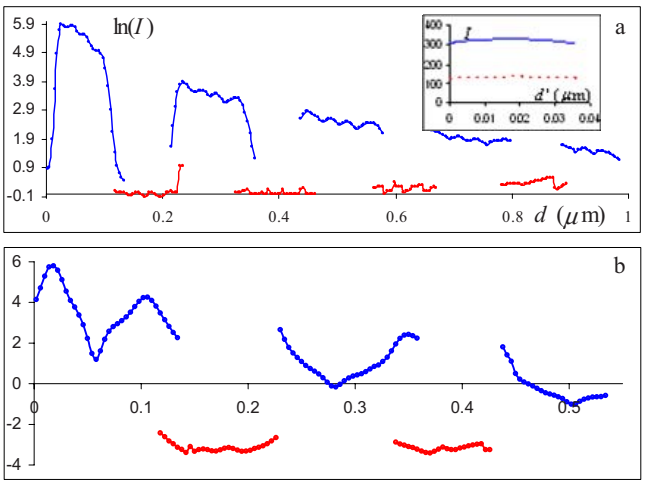

FIG. 6. (Color online) Plots of the light wave intensity (logarithmic) on defect mode wavelength λ^d for the (a) RCP and (b) LCP light versus defect layer thickness d. Parameters are the same as in Fig. 3.

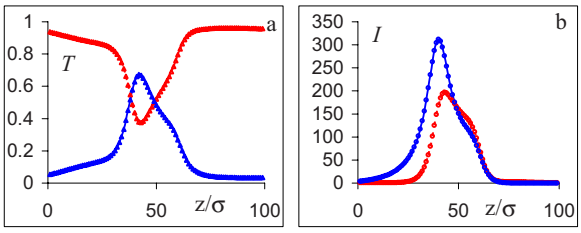

FIG. 7. (Color online) Plots of the (a) transmittance T and (b) intensity I at the defect center on the defect position in the system z/σ for the LCP (the red dotted curve) and RCP (the blue solid curve) light. $\lambda=0.6161$ μm, $d=0.028$ μm. Other parameters are the same as in Fig. 2.

$$\bar{n}^d d = \left(m+\frac{1}{2}\right)\frac{\lambda^d}{2} = \left(m+\frac{1}{2}\right)\frac{\bar{n}\sigma}{2}, \tag{10}$$

where $m=0,1,2,\ldots,\bar{n}=\sqrt{\frac{\varepsilon_{\parallel}+\varepsilon_{\perp}}{2}}$. We also find that the defect mode wavelength approximately is

$$\lambda^d \approx \frac{\lambda_2+\lambda_1}{2} + \frac{\lambda_2-\lambda_1}{2}\cos\left(\frac{2\pi}{\bar{n}\sigma}\bar{n}^d d\right). \tag{11}$$

In Fig. 3(b) the dependence of the defect mode wavelength difference for the normal incident light of the right circular polarization (RCP) and LCP on the defect layer thickness is presented. In Fig. 4 the transmission coefficient's dependence—at the defect mode wavelength—for the incident light—of (a) RCP and of (b) LCP on the defect mode thickness is presented. It is to be noted that we considered both cases $\bar{n}_d>\bar{n}$ and $\bar{n}_d<\bar{n}$.

As it is seen in Fig. 2, if the defect layer thickness is changed, the defect mode bandwidth of incident light of LCP is changed too, and at certain intervals of the defect layer thickness the PBG becomes forbidden for any polarization of incident light [Fig. 2(d)]. *There is a unique effect here: the medium loses its basic optical property, namely, the selectivity in respect to the polarization of the diffraction reflection*. In these thickness intervals of the defect layer the CPCs' polarization dependence of diffraction reflection vanishes and light with every polarization undergoes a diffraction reflection, i.e., becomes independent of the polarization (see Table I). In Fig. 5 the dependence of the defect line half-width—for the incident light of LCP—on the defect layer thickness is presented. The peculiarities described here can be explained as follows. It is known that in Fabry-Perot resonators (including the diffraction ones) the half-widths of the interference band is determined by the reflection coefficients R of the diffraction mirrors $\left(\delta\lambda \propto \frac{\lambda^2(1-R)}{2\pi n^d d\cos\varphi}\right)$, and the number of modes is defined by the defect layer optical thickness. Besides, in this case the defect layer thickness approximately (not exactly) satisfies the condition $d\sim\frac{\lambda}{2(n_e^d-n_o^d)}$, i.e., the defect layer is a half-wave film. And such a film can turn a RCP to the left and vise versa. As a result, in certain ranges of the defect layer changes of two defect modes are aroused, which have a half-width that is large enough—due to the weak reflection at the diffraction mirrors, i.e., these mirrors' reflection coefficients for nonresonance circular polarization are not large—and these modes fill the whole diffraction reflection region.

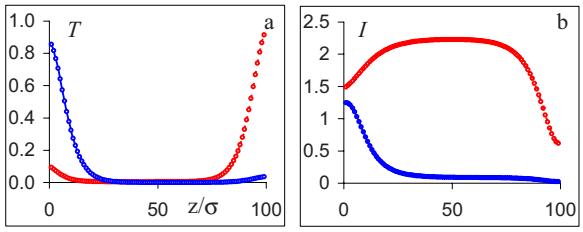

FIG. 8. (Color online). The same dependences as in Fig. 7 at $\lambda=0.625$ μm, $d=1.3$ μm.

As the PBG for a CPC homogeneous layer exists only for one circular polarization, this property is its important advantage in certain practical applications, though this very property is a shortcoming of CPCs in other circumstances. So, the found effect rather widens the possible application range of CPCs.

At further increase of the defect layer thickness the defect mode linewidth of the incident light of LCP decreases [Figs. 2(g)–2(i)]. It is to be noted that the defect mode for incident light of RCP reveals itself as weak-amplitude changes in the reflection spectrum [Figs. 2(c)–2(l) and Fig. 4(a)]. The further increase of the defect layer thickness results in increase of the defect mode number [Figs. 2(j) and 2(l)].

Let us also note that this defect mode number increase can be reached by insertion of multiple but thin layers, as it was shown in [31].

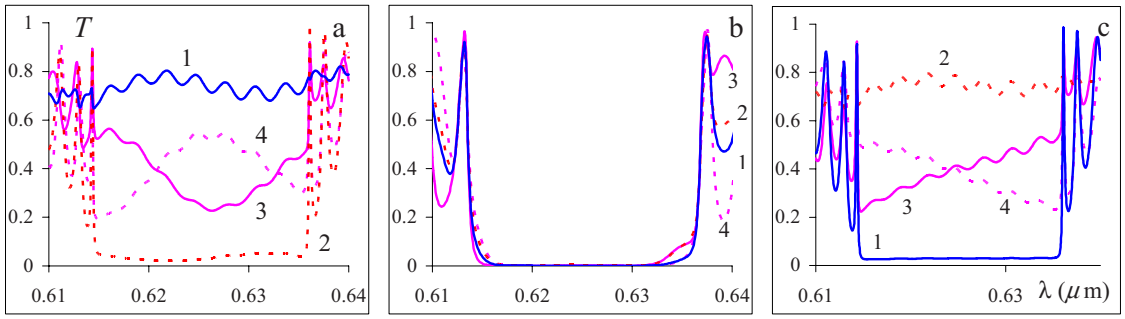

FIG. 9. (Color online) Plots of the transmittance T versus wavelength λ for the incident light, having RCP (1) and LCP (2); and the linear polarizations along the x (3) and y (4) axes directions correspondingly and at different values of z/σ. (a) 5; (b) 50; (c) 95: $d=1.3$ μm.

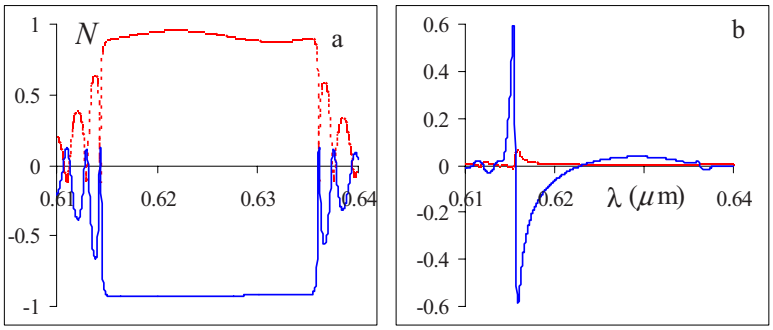

FIG. 10. (Color online) Plots of the nonreciprocity parameter N versus wavelength λ for a right-handed CPC with defect layer thicknesses $d/\sigma \sim 3$ and the location at $z/\sigma=5$ (a), and $d/\sigma \sim 1/10$, and the location at $z/\sigma=20$ (b) are presented. Other parameters are the same as in Fig. 2.

Below we consider in detail the peculiarities of defect modes for the above-mentioned three cases, namely for the small defect layer thickness ($d/\sigma \sim 1/10$); for thicknesses when the diffraction reflection polarization dependence vanishes ($d/\sigma \sim 3$); and for thicknesses when a narrowband defect mode again appears—for LCP ($d/\sigma \sim 5$).

The results of the influence of the defect layer optical axis orientation on defect mode peculiarities were considered in [25]. It is shown there that optical axis orientation change results both in the defect mode wavelength change and in the reflection change at the defect mode wavelengths, and these changes are rather significant. And as in the application it is possible to tune the defect's optical axis orientation—for instance, by means of external fields—so it is possible to improve tunability of the defect modes of these systems.

As it is noted in the Introduction, the defect modes can be used to build low-threshold lasers. In papers [32,33] it is shown that the scaled spontaneous emission rate p is given as

$$p(\lambda,z) = \frac{\rho_m(\omega)}{\rho_{riso}} \frac{\langle |\mathbf{d}|^2 \rangle |E_m(z)|^2}{U(k)}, \tag{12}$$

where ρ_m and $E_m(z)$ are the density of states (DOS) and electric modal field associated to the mth eigenmode, ρ_{iso} is the DOS of an infinite homogeneous slab of constant refractive index, $\langle |\mathbf{d}|^2 \rangle$ is averaged over the orientational distribution transition dipole moment, and $U(k)$ is the total electric energy stored in CPC. Hence, the investigation of light energy distribution in the system is of high interest. This investigation also is important from the other point of view, namely, from the possibility of storage of light energy. In Fig. 6 the (logarithmic) dependence of the light wave intensity of the defect mode—calculated at the defect center—i.e., $\ln(I)=\ln(|E(z=z_d)|^2)$ on the defect layer thickness for Fig. 6(a) LCP and Fig. 6(b) RCP incident light is presented. As it is seen from this figure, essential light energy accumulation in the defect layer takes place at a small defect layer thickness ($d/\sigma \sim 1/10$ at the given parameters of the problem). If this thickness increases, the intensity I rapidly decreases, and for the incident light with RCP this decrease takes place much more rapidly. In the insets the distribution of light energy I inside the defect for the RCP light (the blue solid curve) and LCP light (the red dotted curve) are presented.

Now we consider the influence of the defect layer position changes on defect mode peculiarities. In Fig. 7 the dependence of the transmittance T [Fig. 7(a)] and intensity I at the defect center [Fig. 7(b)] on the defect position in the system (on z/σ) for the incident light with a LCP (the red dotted curve) and RCP (the blue solid curve) in the case of a small defect layer thickness ($d/\sigma \sim 1/10$) is presented, and it is seen that resonance circularly polarized light tunneling and resonance reflection of the light with nonresonance circular polarization take place in the case when the defect is nearby the center (but not at the center), and these curves have certain asymmetry. Much light accumulation also takes place if the defect is nearby the center of the system. In this case, when the defect is nearby the borders of the system (particularly, nearby the right-hand border, as it could be expected) the influence of the defect is practically unobservable.

In Fig. 8 similar dependences are presented at those defect layer thicknesses when the polarization dependence of the diffraction reflection vanishes (at $d/\sigma \sim 3$). If the defect is nearby the right border of the system, the system completely transmits the light with RCP and completely reflects the light with LCP. And if the defect is nearby the left border of the system, the reverse phenomenon is observed, namely, it completely lets through the light with the LCP and completely reflects the right-hand one. And, as we already noted above, if the defect is nearby the center, the system reflects light with any polarization. The transmittance spectra for various z/σ at $d/\sigma \sim 3$ are presented in Fig. 9. To understand their peculiarities let us note the following. As it is known, diffraction reflection of CPC does not change the handedness of circular polarization of light, while homogeneous isotropic (or anisotropic) media turn the handedness to the reverse one when reflecting it. Besides, if light transmits through an anisotropic crystal, additional phase difference appears and due to this fact in the general case of the incidence of circularly polarized waves the transmitted wave generally has elliptical polarization and, as it is mentioned above, the defect layer thickness approximately satisfies the half-wave film condition in this case. Let us note also that in this case we have an

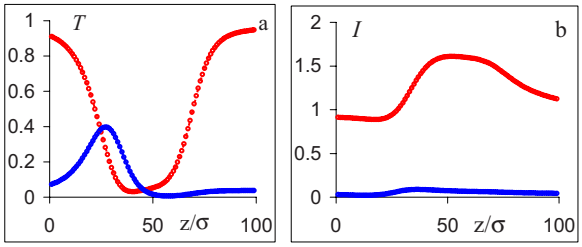

FIG. 11. (Color online) The same dependences as in Fig. 7 at $\lambda=0.6281$ μm, $d=2.8$ μm.

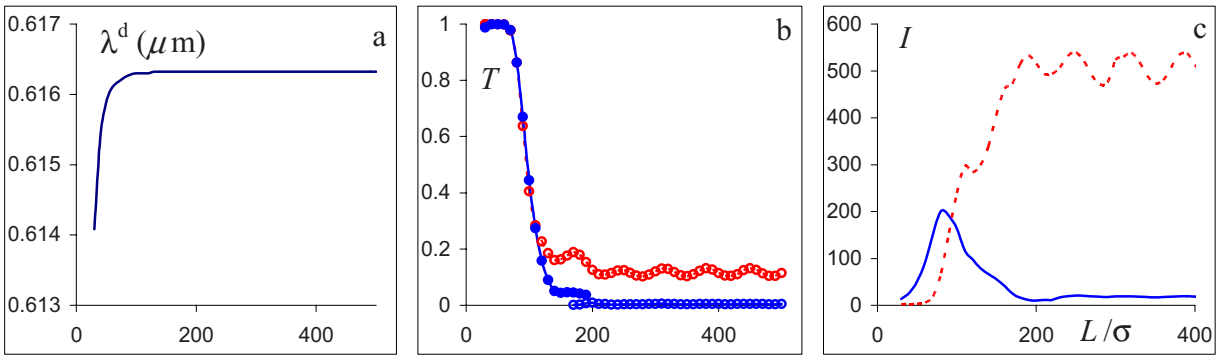

FIG. 12. (Color online) Plots of (a) defect mode wavelength λ^d, (b) transmittance T, and (c) intensity I at the defect center versus CPC thickness (L/σ) are presented. $d=0.028$ μm. Other parameters are the same as in Fig. 2.

asymmetric Fabri-Perot diffraction resonator having selective reflection (transmission) peculiarity in respect to circular polarizations.

These peculiarities of CPC with defect can be used to create sources of elliptically polarized light with tunable ellipticity. Indeed, for instance, for cholesteric liquid crystals (CLC) it is possible to create an anisotropic defect and tune the position of the defect by a static external electric field. Building tandem of electrodes with linear size of $d\sim 3\sigma$ along the CLC axis and consecutively connecting them to a voltage, one can move the defect along the axis of the medium from the right border to the left one, and it will make it possible to tune the ellipticity of the reflected and transmitted signals. If the defect is moved from one border of the system to the other, the ellipticity of the polarization of reflected (or transmitted) signals will change from −1 to +1. Furthermore, the polarization plane rotation of the transmitted light depending on the defect position shows that the rotation practically changes linearly in respect to the change of position of the defect. This peculiarity can have certain applications, too, for instance, in isolators for tuning the polarization plane rotation.

In many electric devices, a diode is an essential component that transmits current in the forward direction but prevents it in the backward direction. The possibility of achieving an anisotropic transmission through a passive optical element is useful in the field of optical isolation and all-optical processing. An optical diode (OD) is defined as a device that permits light in one direction and blocks it in the reverse direction [13,34–37]. Various ODs based on PC structures have been proposed and demonstrated [34–44]. The diode behavior depends on the properties of complex asymmetric structures, different nonlinear materials, left-handed media and polarization converters. As it follows from the above-said the optical system described here can also work as an OD. As calculations show—in particular at $d/\sigma \sim 3$—the system can work as a broadband OD. If nonreciprocal transmittance is described by the parameter $N=\frac{T^+-T^-}{T^++T^-}$ (T^+, T^- are transmission coefficients in the "forward" and "backward" directions), then $N\sim 0.93$ in PBG. And this system can work as a narrow-band OD at $d/\sigma\sim 1/10$. In Fig. 10 the spectra of N of the right-hand (the blue solid curve) and left-hand (the red dotted curve) circularly polarized light incidence on a system with anisotropic defect layer thickness $d/\sigma\sim 3$ located at $z/\sigma=5$ [Fig. 10(a)] and with $d/\sigma=1/10$ located at $z/\sigma=20$ [Fig. 10(b)] are presented.

It seems completely realistic to carry out such systems. For instance, if one made up an anisotropic defect layer in CLC by means of a static external electric field, the defect layer thickness—and also the electrode lengths—would be ~ 3 μm provided $d/\sigma\sim 3$; besides, the applied voltage was to be ~ 500 V, and $E_{cr}\sim 5\times 10^5$ V/m (E_{cr} is the critical electric field at which the molecules of CLC are arranged along that field). Also, the CLC layer thickness was to be $L\sim 100\sigma\sim 42$ μm. Then one could additionally govern the defect layer thickness by the change of the applied voltage.

The investigations of optical devices analogous to electrotechnical ones (diodes, transistors, etc.) have become very important, particularly, because recently a vigorous transition from electric signals to optical ones has been observed, due to vast possibilities of optical signals.

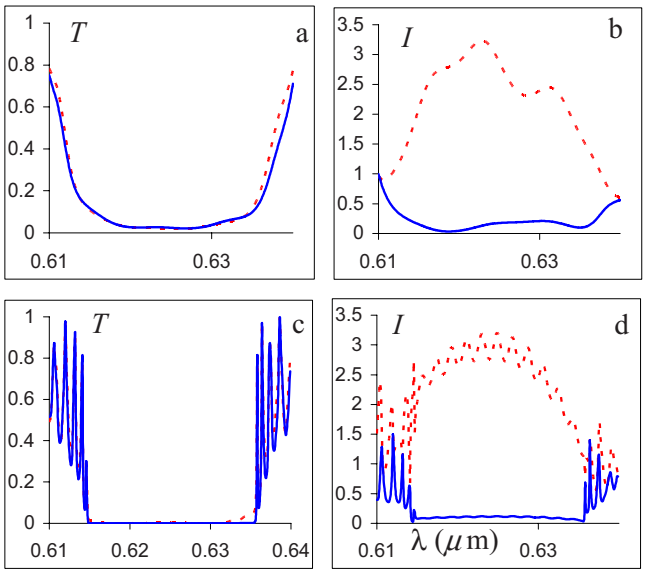

FIG. 13. (Color online) Plots of the (a),(c) transmittance T and (b),(d) intensity I at the defect center versus wavelength λ at various thicknesses of the CPC. (a),(b) $L/\sigma=25$; (c),(d) $L/\sigma=50$. $d=1.3$ μm.

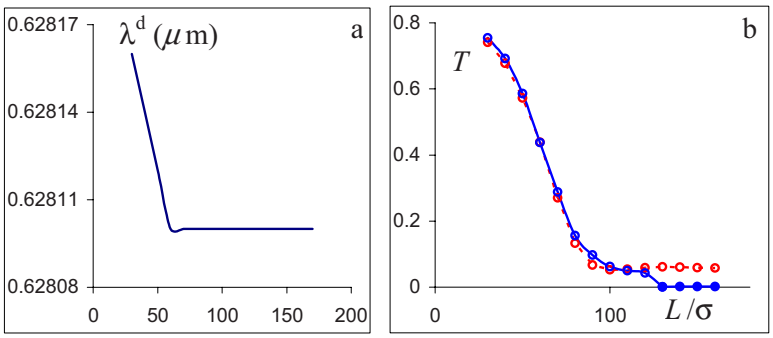

FIG. 14. (Color online) Plots of (a) defect mode wavelength λ^d and (b) transmittance T versus CPC thickness (L/σ) are presented. $d=2.8$ μm. Other parameters are the same as in Fig. 2.

In Fig. 11 (as in Fig. 8) similar dependences are presented for those defect layer thicknesses when again one narrow-band defect mode is observed (it takes place in the case $d/\sigma \sim 5$). As it is seen from the figure, something happens here—in contrast to the case when the defect is at the center of the system—if the defect moves to the left edge of the system, a possibility of tunneling of the light with resonance circular polarization appears (i.e., the transmittance of the light with resonance circular polarization significantly increases), also for these (large) defect thicknesses.

The CPC itself also influences the defect modes. The increase of the CPC thickness results in the decrease of defect mode linewidths. In Fig. 12 the dependences [Fig. 12(a)] of the defect mode wavelength, [Fig. 12(b)] the transmittance coefficient at the defect mode wavelength, and [Fig. 12(c)] the intensity I at the defect center of the defect mode wavelength, on the CPC thickness are presented [below, we characterize the thickness of the chiral PC layer by the number $N=L/\sigma$ of director turns along the film normal ("reduced thickness")]. The defect is at the center of the system, and the defect thickness satisfies the condition $d/\sigma \sim 1/10$. It follows from the presented results that the tunneling of the light with RCP (the blue solid curve) takes place in the case when the CPC thickness is not too large $(L/\sigma \leq 170)$. At larger thicknesses the tunnel transmittance is practically absent, and the defect mode for the RCP of the incident wave reveals itself as weak amplitude changes in the reflection spectrum. Much light accumulation for the resonance polarization of the incident wave also takes place at small thicknesses of the CPC. For the LCP incident wave (the red dotted curves) T and I reach a saturation—oscillating round their certain values if L/σ increases.

In Fig. 13 the dependences of the transmittance T—Figs. 13(a) and 13(c)—and the intensity at the defect center—Figs. 13(b) and 13(d)—on the wavelength λ at various thicknesses of the CPC are presented, assuming, that $d/\sigma \sim 3$, i.e., when the polarization dependence of diffraction reflection vanishes.

In Fig. 14 the dependences [Fig. 14(a)] of the defect mode wavelength and [Fig. 14(b)] of the transmittance T at the defect mode wavelength on CPC thickness (on L/σ) are presented. The defect thickness satisfies the condition $d/\sigma \sim 5$. It follows from the presented results that the tunneling of the light with RCP in this case takes place at much less thickness of the CPC $(L/\sigma \leq 90)$. At larger thicknesses the tunnel transmittance is absent, and the defect mode for the RCP incident wave reveals itself in the form of weak-amplitude changes in the reflection spectrum. For the light with LCP of the incident light T also reaches a saturation if L/σ increases—significantly faster than in the case $d/\sigma \sim 1/10$ (also oscillating round its certain value). In this case I is on the order of 1.5 for the light with LCP of the incident wave, and it is ≤ 0.1 for the light with RCP, i.e., one can consider that light accumulation practically does not take place.

IV. CONCLUSIONS

Concluding, let us note that we have investigated the peculiarities of chiral PC with an anisotropic defect that provides an additional degree of freedom for tuning the defect modes. We found out a unique effect of losing the polarization dependence of diffraction reflection for certain thicknesses of the defect layer. It was found that by tuning the defect layer position one can obtain a source of light with elliptical polarization with tunable polarization. We have shown that large light accumulation at the defect mode takes place either for comparatively smaller thickness of the defect layer, or for comparatively smaller thickness of the CPC itself. In certain conditions, the system can work as an optical diode, which practically completely transmits light in one direction and completely prevents its propagation in the reverse direction.

Finally, let us note that Hodgkinson *et al.* [45] experimentally investigated the transmission spectra of the system: dielectric thin-film helicoidal bianisotropic medium layer—half-wave plate—substrate, and they showed that this system can operate as a polarization-discriminatory handedness-inverter, and whose discriminatory attributes reverse if the entry and the exit pupils are interchanged. In the same way, Song *et al.* [39] experimentally investigated the reflection spectra of the system: CLC—nematic liquid crystal half-wave plate and they showed that such a system can work as an all-optical diode.

Let us also note that all these experimental results are in accordance to our theoretical results.

ACKNOWLEDGMENT

The authors are grateful to Professor Armen Kocharian of California State University for his help in improving the manuscript and useful remarks.

[1] E. Yablonovitch, Phys. Rev. Lett. **58**, 2059 (1987).
[2] S. John, Phys. Rev. Lett. **58**, 2486 (1987).
[3] J. D. Joannopoulos, R. D. Meade, and J. N. Winn, *Photonic Crystals: Modeling the Flow of Light* (Princeton University Press, Princeton, NJ, 1995).
[4] J. Pendry, J. Mod. Opt. **41**, 209 (1994).
[5] P. G. De Gennes and J. Prost, *The Physics of Liquid Crystals* (Clarendon, Oxford, 1993).
[6] L. J. Hodgkinson *et al.*, Opt. Commun. **184**, 57 (2000).
[7] S. Pursel *et al.*, Polymer **46**, 9544 (2005).
[8] Y.-C. Yang, C. S. Kee, J. E. Kim, H. Y. Park, J. C. Lee, and Y. J. Chon, Phys. Rev. E **60**, 6852 (1999).
[9] I. J. Hodgkinson *et al.*, Opt. Commun. **210**, 201 (2002).
[10] J. Schmidtke and W. Stille, Eur. Phys. J. E **12**, 553 (2003).
[11] I. J. Hodgkinson, Q. Wu, L. DeSilva, M. Arnold, M. W. McCall, and A. Lakhtakia, Phys. Rev. Lett. **91**, 223903 (2003).
[12] A. H. Gevorgyan, J. Contemp. Phys. **40**, 32 (2005).
[13] A. H. Gevorgyan, A. Kocharian, and G. A. Vardanyan, Opt. Commun. **259**, 455 (2006).
[14] V. I. Kopp and A. Z. Genack, Phys. Rev. Lett. **89**, 033901 (2002).
[15] J. Schmidtke, W. Stille, and H. Finkelmann, Phys. Rev. Lett. **90**, 083902 (2003).
[16] M. Becchi, S. Ponti, J. A. Reyes, and C. Oldano, Phys. Rev. B **70**, 033103 (2004).
[17] T. Matsui, M. Ozaki, and K. Yoshino, Phys. Rev. E **69**, 061715 (2004).
[18] R. Ozaki *et al.*, Jpn. J. Appl. Phys., Part 1 **45**(1B), 493 (2006).
[19] A. V. Shabanov, S. Ya. Vetrov, and A. Yu. Korneev, JETP Lett. **80**, 181 (2004).
[20] J.-Y. Chen and L.-W. Chen, J. Phys. D **30**, 1118 (2005).
[21] J.-Y. Chen and L.-W. Chen, Phys. Rev. E **71**, 061708 (2005).
[22] J.-Y. Chen and L.-W. Chen, J. Opt. A, Pure Appl. Opt. **7**, 558 (2005).
[23] M. H. Song *et al.*, Adv. Mater. (Weinheim, Ger.) **16**, 779 (2004).
[24] A. Lakhtakia *et al.*, Opt. Commun. **177**, 57 (2000).
[25] A. H. Gevorgyan, Tech. Phys. Lett. **32**, 698 (2006).
[26] V. H. Ambartsumian, J. Phys. (USSR) **8**, 65 (1944).
[27] A. H. Gevorgyan *et al.*, Opt. Spectrosc. **88**, 586 (2000).
[28] A. Lakhtakia and R. Messier, *Sculptured Thin Films: Nanoengineered Morphology and Optics* (SPIE Press, Bellingham, WA, USA, 2005).
[29] A. Lakhtakia, Opt. Commun. **275**, 283 (2007).
[30] G. G. Stokes, Proc. R. Soc. London **11**, 545 (1862).
[31] F. Wang and A. Lakhtakia, Opt. Express **13**, 7319 (2005).
[32] K. L. Woon, M. O'Neill, G. J. Richards, M. P. Aldred, and S. M. Kelly, Phys. Rev. E **71**, 041706 (2005).
[33] J. Schmidtke and W. Stille, Eur. Phys. J. B **31**, 179 (2003).
[34] M. Scalora *et al.*, J. Appl. Phys. **76**, 2023 (1994).
[35] M. Scalora *et al.*, Appl. Phys. Lett. **66**, 2324 (1995).
[36] A. H. Gevorgyan, Tech. Phys. Lett. **29**, 819 (2003).
[37] G. A. Vardanyan and A. H. Gevorgyan, Opt. Spectrosc. **99**, 992 (2005).
[38] J. Hwang *et al.*, Nat. Mater. **4**, 383 (2005).
[39] M. H. Song *et al.*, Thin Solid Films **509**, 49 (2006).
[40] M. H. Song *et al.*, Adv. Funct. Mater. **16**, 1793 (2006).
[41] K. Gallo *et al.*, Appl. Phys. Lett. **79**, 314 (2001).
[42] M. Fujii *et al.*, Opt. Express **16**, 12782 (2006).
[43] M. W. Feise, I. V. Shadrivov, and Yu. S. Kivshar, Phys. Rev. E **71**, 037602 (2005).
[44] J.-Y. Chen and L.-W. Chen, Opt. Express **14**, 10733 (2006).
[45] I. J. Hodgkinson *et al.*, Opt. Eng. (Bellingham) **39**, 2831 (2000).